

# A modified imaging principle for true-amplitude wave-equation migration

D. Kiyashchenko,<sup>1</sup> R.-E. Plessix,<sup>2</sup> B. Kashtan<sup>1</sup> and V. Troyan<sup>1</sup>

<sup>1</sup>State University of Saint-Petersburg, Ulianovskaya street 1, St Petersburg 199504, Russia. E-mail: denis@geo.phys.spbu.ru

<sup>2</sup>Shell International E&P, PO Box 60, 2280 AB Rijswijk, the Netherlands

Accepted 2006 August 18. Received 2006 August 8; in original form 2006 January 13

## SUMMARY

A modified imaging principle is proposed in order to retrieve the ‘true amplitude’ map of the relative slowness perturbations from multishot surface seismic data. The purpose is to obtain a method applicable with a finite-difference solution of the wave equation and equivalent to the ray-based migration/inversion approach. The proposed modification consists of multiplying the integrand of the classic Claerbout imaging principle by an angle-dependent factor in order to remove the angle dependency and obtain an estimate of the slowness perturbations. It is demonstrated that in high-frequency asymptotics the proposed modified imaging principle is similar to the ray-based inversion. A numerical example based on a 2-D synthetic marine-type seismic data set and a finite-difference wavefield extrapolation shows the relevance of this modification.

**Key words:** imaging principle, least-squares inverse problem, ray-based migration/inversion, wavefield extrapolation.

## 1 INTRODUCTION

The study of the impedance or reflection coefficient maps obtained from seismic data is a major processing step in seismology and in hydrocarbon exploration. Extracting angle independent impedance variations or angle-dependent reflection coefficients from migrated seismic sections requires an amplitude preserving migration algorithm, also called true-amplitude migration. Many approaches have been developed during the last three decades.

The first approach is probably Claerbout’s imaging principle, Claerbout (1971, 1983). This method is based on a shot gather and provides a common-shot image of the reflection coefficient. The reflection coefficient distribution map is obtained by correlating at any image points the incident wavefield from the source with the backpropagated wavefield of the receiver data. True-amplitude maps are obtained by dividing the correlation with the square of the norm of the incident wavefield. This approach makes no assumption on the forward modelling. In practice, several artefacts appear when the receiver aperture is limited (which is generally the case in practice, see Hertweck *et al.* 2003; Stolk & Symes 2004). With multishot data set, a structural image is computed by stacking overshots. This stack damages the amplitude estimations because of the angle dependency of pre-stack shot-based images. After identifying potential zones of interest in this structural image, an amplitude versus angle analysis of the shot-based pre-stacked image gives an estimate of the medium parameter perturbations. This is the usual practice. However, it could be interesting to directly derive a ‘true-amplitude’ structural image, namely a ‘true-amplitude’ image of the slowness perturbations in the acoustic with constant density case. The goal of this paper is to develop such a shot-based migration formula useable with finite-difference solutions of the wave equation.

Instead of relying on the imaging principle, in eighties, the migration problem has been formulated as an inverse problem, with a least-squares formulation, Tarantola (1984), or with a generalized inverse Radon transform, Beylkin (1985). These approaches lead to a direct estimation of the medium parameter perturbations. Several approaches were developed based on ray-based modelling. This includes Kirchhoff migration, Keho & Beydoun (1988), Schleicher *et al.* (1993), Beylkin’s approach, Beylkin (1985) and Born migration, Bleistein (1987), Lambaré *et al.* (1992) and Thierry *et al.* (1999). Those approaches may estimate either angle-dependent reflection coefficients, or angle-independent impedance contrasts, namely medium parameter perturbations. They have been applied with any type of data gathers, however, they rely on the high-frequency approximation (ray-based modelling) and on a sufficiently dense aperture.

The least-squares approach, Tarantola (1984), is theoretically the most general approach, can handle any kind of acquisition (multishot, sparse acquisition) and can be used with any type of modelling. *A priori* information can be taken into account through a regularization term. It was shown, Lailly (1983), that the gradient of the least-squares misfit between computed and observed data is a migration algorithm. However, the gradient does not recover the true amplitudes. A true-amplitude migration is obtained when the gradient is pre-multiplied by

the inverse of the Hessian (the second derivatives) of the least-squares misfit. Unfortunately, due to the size of the Hessian operator and because it is non-diagonal, it is not feasible to evaluate its inverse, which may limit the interest of the least-squares approach. Several diagonal approximations of the Hessian have been proposed, for instance Chavent & Plessix (1999), Shin *et al.* (2001), Plessix & Mulder (2004). An iterative approach, generally after linearization around a background model, can be formulated leading to the so-called iterative migration and gives an interesting way to handle sparse acquisition geometry for instance, Nemeth *et al.* (1999), Sevink (1996) and Pica *et al.* (1990).

With complex earth structures ray-based migrations taking into account the multipathing have been successfully developed (ten Kroode *et al.* 1994; Operto & Lambare 2000; Operto *et al.* 2003; Xu & Lambare 2004). However, when significant velocity variations occur on the wavelength scale, the high-frequency approximation reaches its limits. It becomes more practical to solve the wave equation with a finite-difference scheme to account for the finite frequency effects. Currently, this limits the choice of true-amplitude migration algorithm and prevents from using the ray-based inversion approach (Bleistein *et al.* 2001), which is the method of choice with the ray modelling to retrieve the medium slowness perturbations. There is thus an interest to adapt the ray-based inversion formula to the finite-difference modelling or to modify the imaging principle.

Joncour *et al.* (2005) proposed an approach to extract from multishot data set the angle-dependent reflection coefficient map with a finite-difference one-way forward modelling. The method, based on the double square root formulation, Claerbout (1983), and the work of Sava & Fomel (2003), consists of a redatuming of the data and an angle ( $\tau$ -p) transform, with the assumption of a locally constant medium.

In this paper, a different point of view is adopted. We proposed a shot-based approach that aims to retrieve the (angle-independent) impedance perturbation map, defined as the difference between the true and smooth slownesses divided by the smooth slowness in the constant density acoustic case. This is achieved by multiplying the integrand of the classic (Claerbout) imaging principle, namely the cross-correlation between the incident and the backpropagated fields, by the cosine square of the reflection angle at the subsurface point, Kiyashchenko *et al.* (2005b). At least for small incidence angles and small slowness contrasts, the reflection coefficient divided by the cosine of the reflection angles gives the normal incidence angle, which is almost equal, up to a scalar that account for the band-limited effect, to the relative slowness perturbation. In this way, this modified imaging principle provides an (almost) angle independent shot-based image corresponding to relative slowness perturbations. The stack over the shots gives then the ‘true amplitude’ structural image. To justify the modification of the imaging principle, the link with the imaging formula of (Bleistein *et al.* 2001) is made under the high-frequency approximation. This link provides a way to slightly adapt the modified imaging principle in order to make it consistent with the result of (Bleistein *et al.* 2001) under the high-frequency approximation and to retrieve the band-limited version of slowness perturbation. In practice, the finite width of source wavelet and aperture limitations affect the migration and the result corresponds to a band-limited perturbation map. The approach presented in this paper is limited to acoustic case, which limits its applicability to small-to-medium offset data set where the amplitudes are not too much depending on the shear contrasts.

The paper is organized as follows. In the next section, the modified imaging principle is presented. Then, the link between the modified imaging principle and the ray-based inversion approach is drawn under the high-frequency assumption and it is shown that the offset-based image is equal to stacking the shot-based and receiver-based images. In the last section, the modified imaging principle is applied to a 2-D synthetic salt example; the modelling is the multi-one-way wavefield extrapolation, Kiyashchenko *et al.* (2005a).

## 2 MODIFIED IMAGING PRINCIPLE FOR MULTISHOT DATA SET

The goal of the modification of the imaging principle is to develop a finite-difference wave-equation migration algorithm that provides the true-amplitude band-limited impedance map from multishot data, namely a true amplitude structural image. The formulation of this paper is valid for purely acoustic data with constant density. This is still the common assumption of the least-squares migration.

The (classic) common-shot imaging principle is defined by

$$I_C(\mathbf{x}_s, \mathbf{x}) = \frac{1}{P(\mathbf{x}_s, \mathbf{x})} \int_{\Omega} d\omega u_i(\mathbf{x}_s, \mathbf{x}, \omega) \overline{u_b(\mathbf{x}_s, \mathbf{x}, \omega)}, \quad (1)$$

with

$$P(\mathbf{x}_s, \mathbf{x}) = \int_{\Omega} d\omega u_i(\mathbf{x}_s, \mathbf{x}, \omega) \overline{u_i(\mathbf{x}_s, \mathbf{x}, \omega)}, \quad (2)$$

where  $u_i(\mathbf{x}_s, \mathbf{x}, \omega)$  is the incident wavefield from the source  $\mathbf{x}_s$ ,  $u_b(\mathbf{x}_s, \mathbf{x}, \omega)$  is the backpropagated wavefield from the receiver data of the shot  $\mathbf{x}_s$ . The integration is carried out over the frequency range,  $\Omega$ .  $P(\mathbf{x}_s, \mathbf{x})$  is the square norm of the incident wavefield. In practice, the real part of the right-hand side should be taken. However, it is assumed that  $\Omega$  is symmetric with respect to the frequency 0 and thus the real part is not needed because  $u_i(\mathbf{x}_s, \mathbf{x}, -\omega) \overline{u_b(\mathbf{x}_s, \mathbf{x}, -\omega)} = u_i(\mathbf{x}_s, \mathbf{x}, \omega) \overline{u_b(\mathbf{x}_s, \mathbf{x}, \omega)}$ . This simplifies the notation.

In the original paper of Claerbout (1971), imaging principle was defined as  $I_C(\mathbf{x}_s, \mathbf{x}) = \int_{\Omega} d\omega \frac{\overline{u_b(\mathbf{x}_s, \mathbf{x}, \omega)}}{u_i(\mathbf{x}_s, \mathbf{x}, \omega)}$ . In practice, definition (1) gives more stable result, and still provides a quantitative imaging.

$I_C(\mathbf{x}_s, \mathbf{x})$  approximates the plane wave reflection coefficient,  $R(\theta)$ , where  $\theta$  is the reflection angle. It is shot-dependent because the reflection angle at the subsurface point  $\mathbf{x}$  depends on  $\mathbf{x}_s$ . Stacking directly the different common-shot images obtained from a multishot data set creates a post-stack image but with distorted amplitudes due to the shot dependency (or angle dependency) of each image. The amplitude behaviour of the post-stack image should be improved if the common-shot imaging principle is modified to recover an almost shot-independent slowness perturbation from a shot gather.

The shot-independent or angle-independent relative slowness perturbation is defined by

$$r(\mathbf{x}) = \frac{\sigma_t(\mathbf{x}) - \sigma_0(\mathbf{x})}{\sigma_0(\mathbf{x})}, \quad (3)$$

where  $\sigma_t$  is the true slowness and  $\sigma_0$  is the smooth (background) slowness. This is the relative slowness perturbation. The background slowness is assumed known and is used in the computation of the incident and backpropagated wavefields.

For small slowness contrasts and not too large reflection angles,  $\theta$ , the reflection coefficient,  $R$ , is defined by (see Appendix A)

$$R(\theta) \simeq \frac{1}{4 \cos^2(\theta)} \frac{\sigma_+^2 - \sigma_-^2}{\sigma_+^2}, \quad (4)$$

with  $\sigma_+$  the slowness above the interface and  $\sigma_-$  the slowness below the interface. An orientation of the interface has been defined because it is assumed that the incident wave is coming from above the interface, from the medium denoted with  $+$ . If the interface is seen from the opposite orientation, the reflection coefficient has an opposite sign.

It can be assumed that the smooth slowness,  $\sigma_0$ , around the interface satisfies

$$\sigma_0 = \frac{\sigma_+ + \sigma_-}{2}. \quad (5)$$

With  $r_+$ , the slowness contrast seen from above the interface and defined by  $r_+ = \frac{\sigma_+ - \sigma_0}{\sigma_0}$ , the approximation of the reflection coefficient reads for small  $r_+$ :

$$R(\theta) \simeq \frac{r_+}{\cos^2 \theta} \approx \frac{R(0)}{\cos^2 \theta}. \quad (6)$$

$R(0) \approx r_+$  is the zero-offset reflection coefficient. As explained above the (classic) imaging principle, eq. (1), approximates  $R(\theta)$ . A multiplication by  $\cos^2 \theta$  of  $u_i \bar{u}_b$  inside the integral shall then give an approximation of the slowness contrast,  $r_+$ . When the modelling is based on a finite-difference solution of the wave equation the reflection angle  $\theta$  is unknown.  $\cos^2(\theta)$  needs to be defined with the quantities computed during a finite-difference modelling.

At each subsurface point, the normal to a virtual reflector is given by the difference between the slowness vector of the incident wavefield and the slowness vector of the backpropagated wavefield. In terms of angles, this gives  $\theta = (\alpha - \beta)/2$  with  $\alpha$  (correspondingly to  $\beta$ ) the angle between the vertical and the slowness vector of the incident (with respect to backpropagated) wavefield at the subsurface point; and

$$2 \cos^2 \theta = 1 + (\sin \alpha \sin \beta + \cos \alpha \cos \beta). \quad (7)$$

The slowness vector is defined by  $k_x/\omega$  and  $k_z/\omega$  in the wavenumber domain and  $\cos(\alpha) = k_z/k$  and  $\sin(\alpha) = k_x/k$ , with  $k_x$ ,  $k_z$  and  $k$  defined during the forward modelling, and  $\cos(\beta) = k_z/k$  and  $\sin(\beta) = k_x/k$ , with  $k_x$ ,  $k_z$  and  $k$  defined during the backward modelling. The high-frequency approximation of the wavefield gives  $u(x, z, \omega) = a(x, z, \omega) e^{i\omega\tau(x, z)}$  with  $a$  the amplitude and  $\tau$  the traveltime. If the spatial derivatives of the amplitude are neglected,  $\frac{\partial}{\partial x} u \approx i\omega \frac{\partial \tau}{\partial x} u = ik_x u$  since  $k_x = \omega \frac{\partial \tau}{\partial x}$  and  $\frac{\partial}{\partial z} u \approx ik_z u$ . Thus formally in eq. (7),  $\sin$  can be replaced by  $\frac{1}{ik} \frac{\partial}{\partial x}$  and  $\cos$  by  $\frac{1}{ik} \frac{\partial}{\partial z}$ . This leads to the modified imaging principle:

$$I_M^+(\mathbf{x}_s, \mathbf{x}) = \frac{1}{P(\mathbf{x}_s, \mathbf{x})} \int_{\omega} d\omega \left[ u_i(\mathbf{x}_s, \mathbf{x}, \omega) \bar{u}_b(\mathbf{x}_s, \mathbf{x}, \omega) - \frac{1}{k^2} \left( \frac{\partial u_i(\mathbf{x}_s, \mathbf{x}, \omega)}{\partial x} \frac{\partial \bar{u}_b(\mathbf{x}_s, \mathbf{x}, \omega)}{\partial x} + \frac{\partial u_i(\mathbf{x}_s, \mathbf{x}, \omega)}{\partial z} \frac{\partial \bar{u}_b(\mathbf{x}_s, \mathbf{x}, \omega)}{\partial z} \right) \right], \quad (8)$$

$I_M^+(\mathbf{x}_s, x)$  is a common-shot formula and it is an approximation of zero-offset reflection coefficient. This is not the slowness perturbation,  $r(\mathbf{x})$ , defined in eq. (3).

The modified imaging principle formula was derived assuming no multipathing. However, it may work even in the case of multipathing. Indeed, consider  $N$  incident waves at the interface point  $\mathbf{x}$  with traveltimes  $\tau_i$  and (complex) amplitudes  $A_i$ ,  $i = 1, \dots, N$ . The incident wave field is given by formula:  $u_i = \sum_{i=1}^N A_i \exp(i\omega\tau_i)$ . If all the reflected waves are present in the backpropagated field (which is not always the case due to limited aperture),  $u_b = \sum_{i=1}^N A_i R_i \exp(i\omega\tau_i)$ , with  $R_i$  the reflection coefficients. Inserting these expressions into eq. (8) and taking into account eq. (6) assuming that  $\tau_1 \neq \tau_2 \neq \dots \neq \tau_N$  gives:

$$I_M^+(\mathbf{x}_s, \mathbf{x}) = \frac{1}{\int d\omega \sum_{i=1}^N |A_i|^2} \int d\omega \sum_{i=1}^N |A_i|^2 R_i \cos^2 \theta_i \approx r_+(\mathbf{x}). \quad (9)$$

### 3 RELATION BETWEEN THE MODIFIED IMAGING PRINCIPLE AND RAY-BASED INVERSE FORMULA

Docherty (1991) has shown that under the high-frequency approximation, the classic imaging principle gives the same reflection coefficient estimate as the Kirchhoff migration formula or Bleistein's (Bleistein *et al.* 2001) inversion formula. In this part, we demonstrate that the modified imaging principle gives a similar slowness perturbation result as the inversion formula, after a slight modification to account for the band-limited effect. To carry out the comparison the high-frequency approximation of the modified imaging principle,  $I_M^+$ , is first determined.

The modified imaging principle was obtained by multiplying the integrand of the (classic) imaging principle by  $\cos^2(\theta)$  with  $\theta$  the incidence angle at the interface:

$$I_M^+(\mathbf{x}_s, \mathbf{x}) = \frac{1}{P(\mathbf{x}_s, \mathbf{x})} \int_{\Omega} d\omega u_i(\mathbf{x}_s, \mathbf{x}, \omega) \overline{u_b}(\mathbf{x}_s, \mathbf{x}, \omega) \cos^2[\theta(\mathbf{x})]. \tag{10}$$

If the source function is ignored, the incident field,  $u_i(\mathbf{x}_s, \mathbf{x}, \omega)$ , is equal to the Green's function  $G(\mathbf{x}, \mathbf{x}_s, \omega)$ , which satisfies  $\omega^2 \sigma_0^2(\mathbf{x}) G(\mathbf{x}, \mathbf{y}, \omega) + \Delta G(\mathbf{x}, \mathbf{y}, \omega) = -\delta(\mathbf{x} - \mathbf{y})$ . The far-field high-frequency 2-D Green's function can be approximated by (assuming no multipathing)

$$G(\mathbf{x}, \mathbf{y}, \omega) = \frac{e^{i\frac{\pi}{4} \text{sgn}\omega}}{\sqrt{|\omega|}} A(\mathbf{x}, \mathbf{y}) e^{i\omega\tau(\mathbf{x}, \mathbf{y})}. \tag{11}$$

$A$  is the amplitude and  $\tau$  the traveltime.  $\text{sgn}$  is the sign function.

The square of the norm of the incident field is then:

$$P(\mathbf{x}_s, \mathbf{x}) = A^2(\mathbf{x}_s, \mathbf{x}) \int_{\Omega} \frac{d\omega}{|\omega|}. \tag{12}$$

The backpropagated field,  $u_b$ , can be expressed from the representation theorem (see Aki & Richard 1980; Docherty 1991) :

$$\overline{u_b}(\mathbf{x}_s, \mathbf{x}, \omega) \approx 2 \int_{\Sigma_r} d\mathbf{x}_r \frac{\partial G(\mathbf{x}, \mathbf{x}_r, \omega)}{\partial z} \overline{d}(\mathbf{x}_s, \mathbf{x}_r, \omega), \tag{13}$$

where  $d(\mathbf{x}_s, \mathbf{x}_r, \omega)$  is the data due to the shot located at  $\mathbf{x}_s$  and recorded at  $\mathbf{x}_r$  and  $\Sigma_r$  is the receiver acquisition line. This formulation of the representation theorem is based on two assumptions, first, source and receivers are in an infinite medium; secondly, the high frequency assumption applies.

Under the high frequency approximation and assuming only one event in the Green's function, from eq. (11), one obtains

$$\frac{\partial G(\mathbf{x}, \mathbf{x}_r, \omega)}{\partial z} = i\omega \frac{\partial \tau(\mathbf{x}, \mathbf{x}_r)}{\partial z} G(\mathbf{x}, \mathbf{x}_r, \omega). \tag{14}$$

Using the relation (see Appendix B)

$$\cos^2(\theta(\mathbf{x})) \frac{\partial \tau(\mathbf{x}, \mathbf{x}_r)}{\partial z} = \frac{v_0^2(\mathbf{x}) |h(\mathbf{x}_r; \mathbf{x})|}{16\pi A^2(\mathbf{x}_r, \mathbf{x})}, \tag{15}$$

the high-frequency approximation of  $I_M^+$  is:

$$I_M^+(\mathbf{x}_s, \mathbf{x}) = \left( -8\pi \int_{\Omega} \frac{d\omega}{|\omega|} \right)^{-1} \int_{\Sigma_r} \int_{\Omega} d\mathbf{x}_r d\omega \frac{v_0^2(\mathbf{x}) |h_s(\mathbf{x}_r, \mathbf{x})|}{A_d(\mathbf{x}_s, \mathbf{x}, \mathbf{x}_r)} e^{i\omega\tau_d(\mathbf{x}_s, \mathbf{x}, \mathbf{x}_r)} \overline{d}(\mathbf{x}_s, \mathbf{x}_r, \omega), \tag{16}$$

with

$$\begin{cases} \tau_d(\mathbf{x}_s, \mathbf{x}, \mathbf{x}_r) = \tau(\mathbf{x}_s, \mathbf{x}) + \tau(\mathbf{x}_r, \mathbf{x}); \\ A_d(\mathbf{x}_s, \mathbf{x}, \mathbf{x}_r) = A(\mathbf{x}_s, \mathbf{x}) A(\mathbf{x}_r, \mathbf{x}). \end{cases} \tag{17}$$

$h_s$  is the common-shot Beylkin determinant and  $v_0 = 1/\sigma_0$ .

$I_M^+$  is very similar to the common-shot ray-based inverse formula (eq. 5.1.10 of Bleistein *et al.* 2001)

$$\check{r}(\mathbf{x}) = \frac{i}{8\pi^2} \int_{\Sigma_r} \int_{\Omega} d\mathbf{x}_r d\omega \frac{\text{sgn}(\omega) v_0^2(\mathbf{x}) |h_s(\mathbf{x}_r, \mathbf{x})|}{A_d(\mathbf{x}_s, \mathbf{x}, \mathbf{x}_r)} e^{i\omega\tau_d(\mathbf{x}_s, \mathbf{x}, \mathbf{x}_r)} \overline{d}(\mathbf{x}_s, \mathbf{x}_r, \omega). \tag{18}$$

In Bleistein *et al.* (2001) the formula is given for  $\frac{\sigma_r^2(\mathbf{x}) - \sigma_0^2(\mathbf{x})}{\sigma_0^2(\mathbf{x})}$  which is close to  $2r(\mathbf{x})$  for small contrasts, and then the factor  $\frac{1}{8}$  is replaced by  $\frac{1}{4}$ .

Eqs (18) and (16) only differ by the factor  $-\frac{i \text{sgn}\omega}{\pi} \int_{\Omega} \frac{d\omega}{|\omega|}$ . In order to obtain an equivalent of the ray-based inverse formula for the finite-difference wave-equation migration, the integrand in eq. (8) is multiplied by the above factor:

$$I_M(\mathbf{x}_s, \mathbf{x}) = \frac{-i \int_{\Omega} \frac{d\omega}{|\omega|}}{\pi P(\mathbf{x}_s, \mathbf{x})} \int_{\Omega} d\omega \text{sgn}(\omega) \left( u_i(\mathbf{x}_s, \mathbf{x}, \omega) \overline{u_b}(\mathbf{x}_s, \mathbf{x}, \omega) - \frac{1}{k^2} \left[ u_i(\mathbf{x}_s, \mathbf{x}, \omega) \frac{\partial \overline{u_b}(\mathbf{x}_s, \mathbf{x}, \omega)}{\partial x} + \frac{\partial u_i(\mathbf{x}_s, \mathbf{x}, \omega)}{\partial z} \frac{\partial \overline{u_b}(\mathbf{x}_s, \mathbf{x}, \omega)}{\partial z} \right] \right). \tag{19}$$

This modified imaging principle now gives an estimation of the true-amplitude band-limited slowness perturbation as the ray-based inverse formula does. Formula (19) can be implemented with any kind of finite-difference modelling.

It is interesting to recall that under the high-frequency approximation and with a shot gather with infinite aperture, the ray-based inverse formula of Bleistein *et al.* (2001) is the least-square solution. Indeed, with  $F$  the Born mapping, the data are given by  $d = Fr$ . Beylkin (1985), found the true-amplitude common-shot migration by interpreting  $F$  as a generalized Radon transform and by taking the inverse of this generalized Radon transform, namely  $r = F^{-1}d$ ,  $F^{-1}$  exists because  $F$  is a one-to-one map when the aperture and the frequency range are infinite. Bleistein retrieved this result by searching  $B$  such that  $r = Bd$ . Obviously  $B = F^{-1}$ ,  $F^{-1} = (F^*F)^{-1} F^*$ , then  $F^*Fr = F^*d$ .  $r$  satisfies the normal equation associated with the least-squares misfit  $\frac{1}{2} \|Fr - d\|^2$  and then is the least-squares solution. This result has been derived by ten Kroode *et al.* (1994) with the use of the pseudo-differential operator theory (see also Appendix C).

Lambaré *et al.* (1992) noticed that the minimization of a specially weighted misfit function leads to a modified least-squares problem with a diagonal Hessian under the high-frequency approximation. They then proposed an efficient ray-based iterative migration scheme.

Similar idea was used by Sevink (1996), who considered a ray-based Born inversion operator as an equivalent of the least-squares inverse. These two approaches rely on ray-based calculations. The equivalence of Beylkin's and Bleistein's formulas to the least-squares solution justifies the approach of Sevink (1996) and Lambaré *et al.* (1992). The equivalence of the modified imaging principle and the least-squares solution tells that a similar iterative migration approach can be formed with a finite-difference modelling and the modified migration formula (19).

#### 4 THE MULTISHOT MIGRATION FORMULA

The common-shot slowness perturbation image obtained from eq. (19) is less dependent on the shot position than the reflection coefficient map of the classic imaging principle, eq. (1), which intrinsically depends on the shot position. The post-stack slowness perturbation image,  $r_s$ , from a multishot data set can then be simply obtained by stacking the common-shot images over the shots:

$$r_s(\mathbf{x}) = \int_{\Sigma_s} d\mathbf{x}_s I_M(\mathbf{x}_s, \mathbf{x}). \quad (20)$$

$\Sigma_s$  is the source line. The subscript  $s$  in  $r_s$  means that the stack is over the shots. In practice, it is possible to normalize the image by the offset range (or source or receiver range). We ignore this multiplication factor here. Eq. (20) is the shot-based post-stack image.

The modified imaging principle assumes an infinite aperture. In practice, artefacts appear in the pre-stack image due to the limited aperture of the data, see Hertweck *et al.* (2003). With the ray methods, the problem is often overcome by working with the common-offset gathers or common-midpoint gathers. The offset is defined as the difference between the source and the receiver position, and the midpoint corresponds to the point located at the middle between the source and the receiver. The artefacts in the midpoint migrated section are generally reduced because each data trace of a midpoint gather more or less illuminates the same part of the earth, under the assumption that the lateral changes in the earth are mild compared to the vertical changes. The high-frequency offset-based post-stack image,  $r_o$ , is

$$r_o(\mathbf{x}) = \frac{i}{8\pi^2} \int_{\Sigma_o} \int_{\Sigma_h} \int_{\Omega} d\mathbf{x}_o d\mathbf{x}_h d\omega \frac{\text{sgn}(\omega) v_0^2(\mathbf{x}) |h_o(\mathbf{x}_o, \mathbf{x}_h; \mathbf{x})|}{A_d(\mathbf{x}_o; \mathbf{x}, \mathbf{x}_h)} e^{i\omega\tau_d(\mathbf{x}_o; \mathbf{x}, \mathbf{x}_h)} \bar{d}(\mathbf{x}_o; \mathbf{x}_h, \omega). \quad (21)$$

$\mathbf{x}_h = \frac{\mathbf{x}_s + \mathbf{x}_r}{2}$  is the midpoint,  $\mathbf{x}_o = \frac{\mathbf{x}_s - \mathbf{x}_r}{2}$  is the offset,  $h_o$  is the offset Beylkin determinant.  $\Sigma_h$  is the midpoint line and  $\Sigma_o$  is the offset line. This formula is obtained by integrating the common-offset images over the offsets. The result may be normalized by offset range.

A common-offset image requires the computation of the Green's functions from the sources located at  $\mathbf{x}_h + \mathbf{x}_o$  and from the receivers located at  $\mathbf{x}_h - \mathbf{x}_o$ . For the post-stack image this means that the Green's functions from all the sources and from all the receivers have to be computed independently. With a ray based modelling this does not increase the computation time because they are also computed with a common-shot algorithm. However, it does with a finite-difference modelling. Indeed in the common-shot imaging principle, the Green's functions from each receiver are not computed because the whole backpropagated field can be computed at once with a finite-difference modelling. This makes the offset-based formula unaffordable with a finite-difference solution of the wave equation, except in very particular cases when the Green's functions can be stored. However, it is possible to obtain the offset-based post-stack image without computing the common-offset images.

The offset gather Beylkin determinant,  $h_o$ , is defined by

$$h_o(\mathbf{x}_o, \mathbf{x}_h; \mathbf{x}) = \det \left( \mathbf{p}_s + \mathbf{p}_r, \frac{\partial \mathbf{p}_s + \partial \mathbf{p}_r}{\partial \mathbf{x}_h} \right), \quad (22)$$

with  $\mathbf{p}_s$  the slowness vector at  $\mathbf{x}$  on the ray coming from the source and  $\mathbf{p}_r$  the slowness vector at  $\mathbf{x}$  on the ray coming from the receiver.

Since  $\mathbf{x}_s = \mathbf{x}_o + \mathbf{x}_h$  and  $\mathbf{x}_r = \mathbf{x}_o - \mathbf{x}_h$ ,

$$\frac{\partial \mathbf{p}_s + \partial \mathbf{p}_r}{\partial \mathbf{x}_h} = \frac{\partial \mathbf{p}_s}{\partial \mathbf{x}_s} + \frac{\partial \mathbf{p}_r}{\partial \mathbf{x}_r}. \quad (23)$$

Therefore,

$$h_o(\mathbf{x}_o, \mathbf{x}_h; \mathbf{x}) = h_s(\mathbf{x}_s, \mathbf{x}_r; \mathbf{x}) + h_r(\mathbf{x}_r, \mathbf{x}_s; \mathbf{x}), \quad (24)$$

with  $h_s$  the shot gather Beylkin determinant and  $h_r$  the receiver gather Beylkin determinant.

With the relation between Beylkin's determinant, eq. (24), and the Jacobian,  $|\frac{\partial(\mathbf{x}_s, \mathbf{x}_r)}{\partial(\mathbf{x}_o, \mathbf{x}_h)}| = 2$ , of the coordinate transform between  $(\mathbf{x}_o, \mathbf{x}_h)$  and  $(\mathbf{x}_s, \mathbf{x}_r)$ :

$$r_o(\mathbf{x}) = \frac{1}{2} \left( \int_{\Sigma_s} I_M(\mathbf{x}_s, \mathbf{x}) + \int_{\Sigma_r} I_M(\mathbf{x}_r, \mathbf{x}) \right) = \frac{1}{2} (r_s(\mathbf{x}) + r_r(\mathbf{x})), \quad (25)$$

where  $r_r(\mathbf{x})$  is the receiver-based post-stack slowness perturbation section. It is computed by reordering the data by receiver gathers using the reciprocity theorem. With limited aperture but dense acquisition, for example with a marine-type of acquisition, the post-stack slowness perturbation image obtained from eq. (25) contains less artefacts (migration smiles) than the one obtained from eq. (20) and, therefore, shows a better amplitude estimation (Kiyashchenko *et al.* 2005b). However, applying eq. (25) doubles the computational cost.

## 5 NUMERICAL EXAMPLE

In this section, a migration of a 2-D synthetic marine-type data set is shown. The marine-type synthetic data have been generated with a frequency-domain finite-difference code from the section of a SEG/EAGE salt model shown in Fig. 1. A direct solver of the Helmholtz equation is applied in this modelling code. The acquisition consists of 237 shots, each having 65 receivers with spacing of 40 m. The maximum offset in the data is 2.7 km.

The modelling used in the migration is a wavefield extrapolation method based on the multi-one-way modelling scheme in order to correctly approximate the amplitudes of the wavefield (Kiyashchenko *et al.* 2005a). The background velocity corresponds to a smooth version of the true model. A Gaussian filter was used for the smoothing:  $M_{sm}(x, z) = \frac{\pi}{a^2} \int dx \int dz e^{-\frac{x^2+z^2}{a^2}} M_o(x, z)$ , with  $a = 40$  m, where  $M_o$  is original velocity model and  $M_{sm}$  is its smoothed version.

The true slowness perturbation, Fig. 2, is defined as the difference between the true model and the smooth model divided by the smooth model. The result of the offset-based modified imaging principle, eq. (25), is shown in Fig. 3. Some of the reflectors beneath the salt body, principally the two reflectors touching the right-hand side of the salt body around 2 and 3 km depth, are not recovered due to the limited aperture (2.7 km). Larger offsets are required to retrieve those reflectors. For comparison, the image obtained with the classic imaging principle after stacking over sources and receivers is displayed, Fig. 4.

In order to quantitatively evaluate the amplitude estimates, two vertical slowness perturbation logs are plotted, Figs 5 and 6. The amplitudes of the retrieved slowness perturbations are calibrated to the amplitude of the first reflector. A band-limited true slowness perturbation is plotted for comparison. The filtering was done in the following way; first the perturbation log was transformed to time domain, then convolved with the source wavelet, and finally transformed back to depth domain (see Thierry *et al.* 1999). This filtering is designed to roughly reproduce what should be retrieved after the migration of the finite-frequency and band-limited data. The log in Fig. 5 corresponds to a sedimentary zone on the left of the salt, at  $x = -0.7$  km. In this part the velocity contrasts are small. With the classic imaging principle, the amplitudes of the deeper reflectors are underestimated. Moreover, the log does not represent the slowness perturbation but its derivatives. With the modified imaging principle, up to a multiplicative factor, the migrated perturbation log is a band-limited version of the true slowness perturbation. The errors in the amplitude estimates do not exceed 20 per cent. The amplitude behaviour of the slowness perturbation is well recovered in this case.

The log in Fig. 6 crosses the right part of the salt where the velocity contrast is large (from about 2500 to 4500 m s<sup>-1</sup> in the salt body). With the classic imaging principle the amplitudes of the deeper reflectors are again underestimated. With the modified imaging principle, the amplitudes of almost all reflectors are well recovered. However, the amplitude of the top of the salt body, approximately at 1.5 km, is significantly overestimated. The overestimation of the amplitudes at the salt interfaces may be due to the large velocity contrast and to the angle limitation of the one-way schemes. The reflector at  $z = 2.8$  km is not correctly retrieved because of the finite bandwidth effect. Indeed,

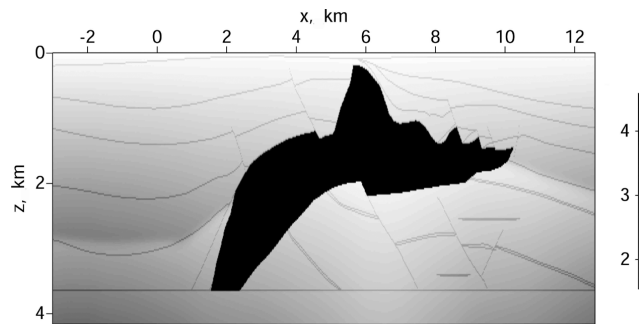


Figure 1. 2-D section of the SEG/EAGE salt model.

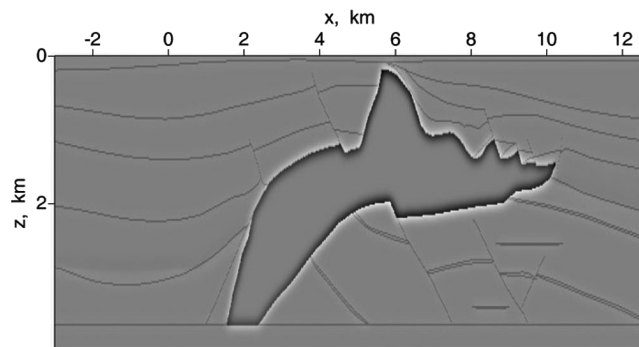
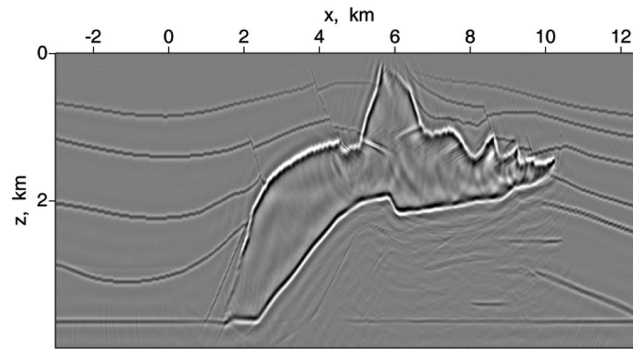
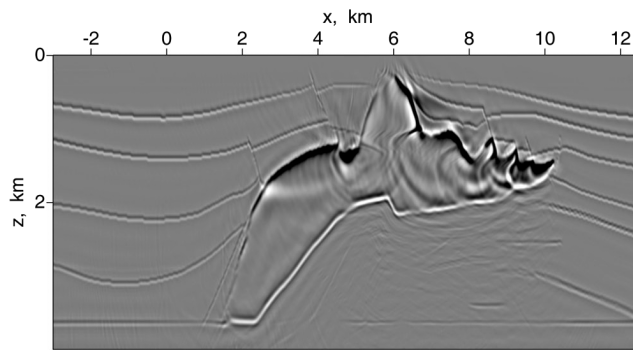


Figure 2. True slowness perturbation of the SEG/EAGE salt model.



**Figure 3.** The migrated slowness perturbation image of the salt model obtained with the modified imaging principle.



**Figure 4.** The migrated slowness perturbation image of the salt model obtained with the classic imaging principle.

it is also hardly visible on the band-limited true slowness log, Fig. 6: the reflectors at 2.8 and 3 km can hardly be distinguished within this frequency band. The errors in the amplitude estimates of other reflectors is less than 30 per cent.

This example shows that the modified imaging principle improves the amplitude of the band-limited slowness perturbation on the post-stack image and it can be used for an amplitude-preserving migration.

## 6 CONCLUSIONS AND DISCUSSIONS

A modified imaging principle has been proposed to migrate a shot gather of a seismic data set using a wave-equation finite-difference solver. This migration gives an amplitude preserving (true) estimation of the band-limited slowness perturbation distribution. The result is less shot-dependent than the one of Claerbout's imaging principle, which approximates the reflection coefficient. Therefore, it is more appropriate for stacking the common-shot images over shots.

Under the high-frequency approximation it was demonstrated that this modified imaging principle is equivalent to the ray-based migration/inversion approach and, therefore, gives the true amplitudes. This formula can be seen as an inversion formula applicable with a finite-difference solution of the wave equation. In practice, shot-based images can show some finite aperture artefacts. To remove some of the aperture effects, shot-based and receiver-based migrated images can be stacked. This provides a post-stack offset-based approach for the wave-equation migration without explicitly computing the common-offset images, which is too expensive with a finite-difference wave-equation modelling. The equivalence can be demonstrated with the high-frequency inverse formula. This approach doubles the cost of the imaging principle.

The 2-D numerical example shows the relevance of this modified imaging principle to retrieve the slowness perturbation from a multishot data set. *A priori*, the formula can be extended to 3-D data sets.

## ACKNOWLEDGMENTS

This work was supported by the grants CRDF RG0-1318(4) and RFBR 05-05-65301. The authors thank Gilles Lambare and anonymous reviewer for their thorough review of the paper and valuable comments.

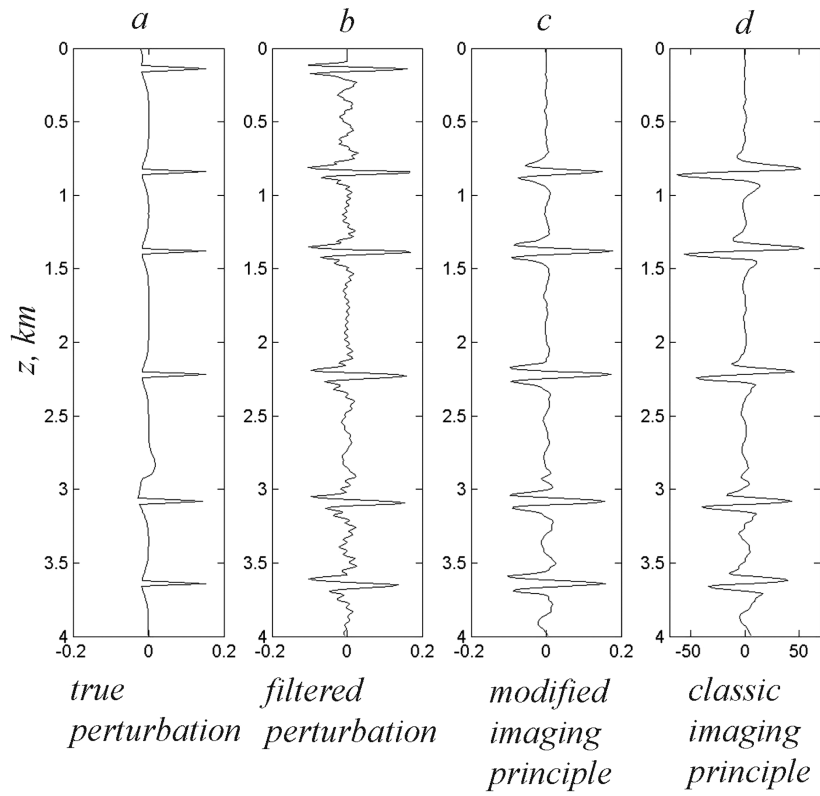


**Figure 5.** Comparison of the true slowness perturbation log (solid line, a) and the migrated slowness perturbation logs at  $x = -0.7$  km. Second graph (b) is filtered slowness perturbation. Third graph (c)—modified imaging principle result. Last graph (d)—classic imaging principle result.

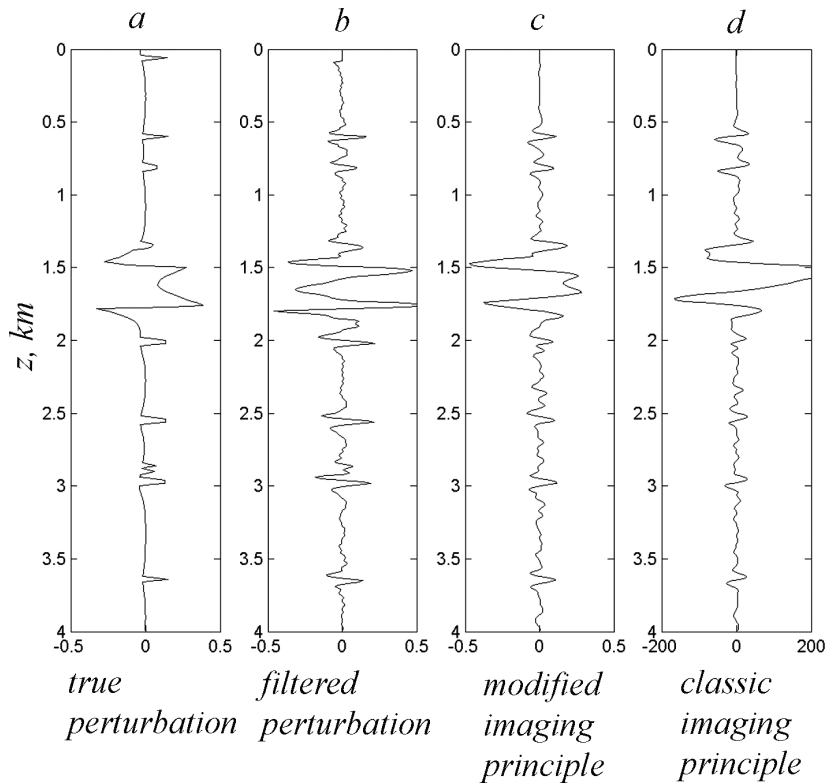


**Figure 6.** Comparison of the true slowness perturbation logs (solid line, a) and the migrated logs at  $x = 9.8$  km. Second graph (b) is filtered slowness perturbation. Third graph (c)—modified imaging principle result. Last graph (d)—classic imaging principle result.

REFERENCES

- Aki, K. & Richard, P.G., 1980. *Quantitative Seismology, Theory and Methods*, Freeman and Company, San Francisco.
- Beylkin, G., 1985. Imaging of discontinuities in the inverse scattering problem by inversion of a causal generalized Randon transform, *J. Math. Phys.*, **26**, 99–108.
- Bleistein, N., 1987. On the imaging of the reflectors in the earth, *Geophysics*, **52**, 931–942.
- Bleistein, N., Cohen, J. & Stockwell J., 2001. *Mathematics of Multi-dimensional Seismic Imaging and Inversion*, Springer, New York.
- Chavent, G. & Plessix, R.-E., 1999. An optimal true amplitude least-squares prestack depth migration, *Geophysics*, **64**, 508–515.
- Claerbout, J.F., 1971. Toward a unified theory of reflector mapping, *Geophysics*, **36**, 467–481.
- Claerbout, J.F., 1983. *Imaging the Earth's Interior*, Blackwell Scientific Publication Co., Boston, MA.
- Docherty, P., 1991. A brief comparison of some Kirchhoff integral formula for migration and inversion, *Geophysics*, **56**, 1164–1169.
- Hertweck, T., Jager, C., Goertz, A. & Schleicher, J., 2003. Aperture effects in 2.5D Kirchhoff migration: a geometrical explanation, *Geophysics*, **68**, 1673–1684.
- Joncour, F., Svay-Lucas, J., Lambaré, G. & Duquet, B., 2005. True amplitude wave equation migration, *EAGE 67th International Conference and Exhibition*, Madrid, Expanded Abstracts.
- Keho, T.H. & Beydoun, B., 1988. Paraxial ray Kirchhoff migration, *Geophysics*, **53**, 1540–1546.
- Kiyashchenko, D., Plessix, R.-E., & Kashtan, B., 2005a. Improved amplitude multi-one-way modeling method, *Wave Motion*, **43**, 99–115.
- Kiyashchenko, D., Plessix, R.-E., Kashtan, B. & Troyan, V., 2005. Improved amplitude multi-one-way migration, *EAGE 67th International Conference and Exhibition*, Madrid, Expanded Abstract.
- Lailly, P., 1983. The seismic inverse problem as a sequence of before stack migration, in *Proc. Conf. on Inverse Scattering, Theory and Application*, SIAM, Philadelphia.
- Lambaré, G., Virieux, J., Madariaga, R. & Jin, S., 1992. Iterative asymptotic inversion in the acoustic approximation, *Geophysics*, **57**, 1138–1154.
- Nemeth, T., Wu, C. & Schuster, G.T., 1999. Least-squares migration of incomplete reflection data, *Geophysics*, **64**, 208–221.
- Operto, S. & Lambaré, G., 2000. Can we quantitatively image complex structure with rays?, *Geophysics*, **65**, 1223–1238.
- Operto, S., Lambaré, G., Podvin, P. & Thierry, P., 2003. 3D ray-Born migration/inversion - Part 2: case study of the SEG/EAGE overthrust experiment, *Geophysics*, **68**, 1357–1370.
- Pica, A., Diet, J. & Tarantola, A., 1990. Nonlinear inversion of seismic reflection data in a laterally invariant medium, *Geophysics*, **55**, 284–292.
- Plessix, R.E. & Mulder, W.A., 2004. Frequency-domain finite-difference amplitude-preserving migration, *Geophys. J. Int.*, **157**, 975–987.
- Sava, P. & Fomel, S., 2003. Amplitude-preserved common gathers by wave-field continuation methods, *Geophysics*, **68**, 1065–1074.
- Schleicher, J., Filpo, E., Hanitzsch, C., Hubral, P. & Tygel, M., 1993. Amplitude-preserving migration using diffraction stacks, *38th. Ann. Int. Mtg., SPIE, Proceedings, Mathematical Methods in Geophysical Imaging*, 97–108. San Diego, CA.
- Sevink, A., 1996. Asymptotic seismic inversion, *PhD thesis*, Delft University of Technology, The Netherlands
- Shin, C., Jang, S. & Min, D., 2001. Improved amplitude preservation for prestack depth migration by inverse scattering theory, *Geophys. Prospect.*, **49**, 592–606.
- Stolk, C. & Symes, W., 2004. Kinematic artifacts in prestack depth migration, *Geophysics*, **69**, 566–575.
- Tarantola, A., 1984. Inversion of seismic reflection data in the acoustic approximation, *Geophysics*, **49**, 1259–1266.
- ten Kroode, A., Smit, D. & Verdel, A., 1994. A microlocal analysis of the migration, *Wave Motion*, **28**, 149–172.
- Thierry, P., Operto, S. & Lambaré, G., 1999. Fast 2D ray+Born migration/inversion in complex media, *Geophysics*, **34**, 162–182.
- Treves, F., 1980. *Introduction to Pseudo-differential and Fourier Integral Operators*, Plenum Press, New York.
- Xu, S. & Lambare, G., 2004. Fast migration/inversion with multi-valued ray fields. Part I: method, validation tests and application to 2D Marmousi, *Geophysics*, **69**, 1311–1328.

APPENDIX A: APPROXIMATION OF REFLECTION COEFFICIENT

In this appendix, the approximation of the plane wave reflection coefficient for constant density acoustic and small slowness contrast is briefly retrieved.

Let  $\sigma_+$  (with respect to  $\sigma_-$ ) be the slowness above (with respect to below) the horizontal interface. The incident wave is coming from the domain above the interface with an incident angle  $\theta$  between the wave propagation direction and the normal to the interface. With  $\omega$  the angular frequency, the wavenumbers of the incident and transmitted waves are correspondingly  $k_+ = \omega\sigma_+$  and  $k_- = \omega\sigma_-$ . The reflection coefficient, obtained by assuming continuity of the pressure and particle acceleration at the interface, is equal to:

$$R = \frac{(k_+^2 - k_x^2)^{1/2} - (k_-^2 - k_x^2)^{1/2}}{(k_+^2 - k_x^2)^{1/2} + (k_-^2 - k_x^2)^{1/2}}, \tag{A1}$$

with  $k_x$  the horizontal component of the incident wavenumber vector.  $k_x$  is continuous at the interface.

With  $k_{+z} = \sqrt{k_+^2 - k_x^2}$  and  $k_-^2 - k_x^2 = k_{+z}^2 + k_-^2 k_{+z}^2$ ,  $R$  can be rewritten as follows:

$$R = \frac{1 - \left(1 + \frac{k_-^2 - k_+^2}{k_{+z}^2}\right)^{1/2}}{1 + \left(1 + \frac{k_-^2 - k_+^2}{k_{+z}^2}\right)^{1/2}}. \tag{A2}$$

$k_-^2 k_{+z}^2$  is a small quantity under the assumption of small slowness contrasts. A Taylor development gives:

$$R \simeq \frac{k_+^2 - k_-^2}{4k_{+z}^2}. \tag{A3}$$

The incident angle satisfies  $k_{+z} = k_+ \cos \theta$ . With the relation between the slownesses and the wavenumbers, the approximation of the reflection coefficient is thus equal to:

$$R(\theta) = \frac{1}{4 \cos^2 \theta} \frac{\sigma_+^2 - \sigma_-^2}{\sigma_+^2} \quad (\text{A4})$$

Notice that an orientation of the interface has been defined when it was assumed that the incident wave propagates in the medium denoted +.

## APPENDIX B: BEYLKIN DETERMINANT AND AMPLITUDE TERM

In this appendix, Beylkin's determinant is written with the amplitude of the Green's function and the ray parameters in order to obtain the formula (15).

The Jacobian of the transformation between  $(\xi, \omega)$  and  $\mathbf{k}$  in a 2-D space is

$$\left| \frac{\partial(\mathbf{k})}{\partial(\xi, \omega)} \right| = |\omega| \det \left( \mathbf{p}, \frac{\partial \mathbf{p}}{\partial \mathbf{x}_r} \right), \quad (\text{B1})$$

with  $\mathbf{k} = \omega \mathbf{p}$  and  $\mathbf{p} = \nabla_{\mathbf{x}} \tau(\mathbf{x}, \mathbf{x}_s) + \nabla_{\mathbf{x}} \tau(\mathbf{x}, \mathbf{x}_r) = \mathbf{p}_s + \mathbf{p}_r$ .  $\mathbf{p}_s$  and  $\mathbf{p}_r$  are the slowness vectors of the ray going from  $\mathbf{x}_s$  to  $\mathbf{x}$  and the ray going from  $\mathbf{x}_r$  and  $\mathbf{x}$ . With  $\alpha$  the angle at the subsurface point  $\mathbf{x}$  between the vertical and the slowness vector of the ray from  $\mathbf{x}_s$  and  $\mathbf{x}$ ,  $\beta$  the angle at  $\mathbf{x}$  between the vertical and the slowness vector of the ray from  $\mathbf{x}_r$  and  $\mathbf{x}$ , the slowness vectors satisfy

$$\mathbf{p}_s(\mathbf{x}) = \frac{1}{v_0(\mathbf{x})} \begin{Bmatrix} \sin[\alpha(\mathbf{x})] \\ \cos[\alpha(\mathbf{x})] \end{Bmatrix}; \quad \mathbf{p}_r(\mathbf{x}) = \frac{1}{v_0(\mathbf{x})} \begin{Bmatrix} \sin[\beta(\mathbf{x})] \\ \cos[\beta(\mathbf{x})] \end{Bmatrix}. \quad (\text{B2})$$

Beylkin's determinant,  $h(\mathbf{x}_r; \mathbf{x})$ , is then equal to

$$\begin{aligned} h(\mathbf{x}_r; \mathbf{x}) &= \det \left[ \mathbf{p}(\mathbf{x}), \frac{\partial \mathbf{p}(\mathbf{x})}{\partial \mathbf{x}_r} \right] \\ &= \frac{1 + \cos[\alpha(\mathbf{x})] \cos[\beta(\mathbf{x})] + \sin[\alpha(\mathbf{x})] \sin[\beta(\mathbf{x})]}{v_0^2(\mathbf{x})} \left| \frac{\partial \beta(\mathbf{x})}{\partial \mathbf{x}_r} \right|. \end{aligned} \quad (\text{B3})$$

With  $J$  2-D the Jacobian of the coordinate transform between the Cartesian coordinates  $(x, z)$  and the ray coordinates  $(\beta, \tau)$ :

$$\frac{\partial \beta(\mathbf{x})}{\partial \mathbf{x}_r} = \frac{1}{J_{2-D}} \frac{\partial \tau(\mathbf{x}, \mathbf{x}_r)}{\partial z}. \quad (\text{B4})$$

The amplitude of the Green's function and the Jacobian are related by

$$A(\mathbf{x}, \mathbf{x}_r) = \frac{1}{\sqrt{8\pi} J_{2-D}}. \quad (\text{B5})$$

Since  $2 \cos^2(\theta) = 1 + \cos \alpha \cos \beta + \sin \alpha \sin \beta$ , this means:

$$h(\mathbf{x}_r; \mathbf{x}) = \frac{16\pi \cos^2[\theta(\mathbf{x})] A^2(\mathbf{x}, \mathbf{x}_r)}{v_0^2(\mathbf{x})} \frac{\partial \tau(\mathbf{x}, \mathbf{x}_r)}{\partial z}, \quad (\text{B6})$$

and thus the formula (15).

## APPENDIX C: HIGH-FREQUENCY LEAST-SQUARES SOLUTION

In this appendix, we rederive for completeness the high-frequency least-squares slowness perturbation approximation. This result, in a more general form, can be found in ten Kroode *et al.* (1994). The derivation is quite similar to the work of Beylkin (1985) except that we start here from the normal equation obtained from the least-squares formulation.

The synthetics,  $c$ , under the Born approximation, satisfies, with  $\tilde{r}$  the relative slowness perturbation:

$$c(\xi, \omega) = 2\omega^2 \int_D d\mathbf{x} \sigma_0^2(\mathbf{x}) G(\mathbf{x}, \mathbf{x}_s(\xi), \omega) G(\mathbf{x}, \mathbf{x}_r(\xi), \omega) \tilde{r}(\mathbf{x}). \quad (\text{C1})$$

$\xi$  is the gather parameter and lies on the line  $\Sigma$ . The least-squares misfit,  $J$ , is, for a given observed data gather,  $d_{\text{obs}}(\xi, \omega)$ :

$$J(\tilde{r}) = \frac{1}{2} \int_{\Sigma} \int_{\Omega} d\xi d\omega |d_{\text{obs}}(\xi, \omega) - d_{\text{calc}}(\xi, \omega)|^2, \quad (\text{C2})$$

where  $d_{\text{calc}}$  is the calculated (synthetic) data set.  $J$  is a quadratic function in  $\tilde{r}$ , therefore, the optimal slowness perturbation,  $\check{r}$ , satisfies

$$H\check{r} = -g, \quad (\text{C3})$$

where  $g$  is the gradient of  $J$  evaluated at  $\tilde{r} = 0$  and  $H$  is the Hessian.

Using the approximation of the Green's function, eq. (11), and the notations:

$$\begin{cases} \tau_d(\mathbf{x}, \xi) = \tau(\mathbf{x}_s(\xi), \mathbf{x}) + \tau(\mathbf{x}_r(\xi), \mathbf{x}); \\ A_d(\mathbf{x}, \xi) = A(\mathbf{x}_s(\xi), \mathbf{x}) A(\mathbf{x}_r(\xi), \mathbf{x}); \\ \phi_d(\mathbf{x}, \mathbf{y}, \xi) = \tau_d(\mathbf{y}, \xi) - \tau_d(\mathbf{x}, \xi), \end{cases} \quad (\text{C4})$$

the gradient at  $\tilde{r} = 0$  is:

$$\begin{aligned} g(\mathbf{x}) &= \frac{\partial J}{\partial \tilde{r}(\mathbf{x})} \\ &= -2\sigma_0^2(\mathbf{x}) \int_{\Sigma} \int_{\Omega} d\xi d\omega i\omega A_d(\mathbf{x}, \xi) e^{i\omega\tau_d(\mathbf{x}, \xi)} \bar{d}(\xi, \omega) \end{aligned} \quad (C5)$$

and the Hessian is:

$$\begin{aligned} H(\mathbf{x}, \mathbf{y}) &= \frac{\partial^2 J}{\partial \tilde{r}(\mathbf{x}) \partial \tilde{r}(\mathbf{y})} \\ &= 4\sigma_0^2(\mathbf{y})\sigma_0^2(\mathbf{x}) \int_{\Sigma} \int_{\Omega} \omega^2 d\xi d\omega A_d(\mathbf{x}, \xi) A_d(\mathbf{y}, \xi) e^{i\omega\phi_d(\mathbf{x}, \mathbf{y}, \xi)}. \end{aligned} \quad (C6)$$

(The real part is not taken as explained previously.)

With the Fourier representation  $\check{r}(\mathbf{y}) = \frac{1}{(2\pi)^2} \int_K d\mathbf{k} \check{r}(\mathbf{k}) e^{-i\mathbf{k}\cdot\mathbf{y}}$ , and the integral representation of eq. (C3),  $\int_D d\mathbf{y} H(\mathbf{x}, \mathbf{y}) \check{r}(\mathbf{y}) = -g(\mathbf{x})$ , we obtain

$$\frac{1}{(2\pi)^2} \int_K d\mathbf{k} V_a(\mathbf{k}, \mathbf{x}) \check{r}(\mathbf{k}) = -g(\mathbf{x}), \quad (C7)$$

$K$  is the wavenumber 2-D real space.

$$V_a(\mathbf{k}, \mathbf{x}) = \int_D \int_{\Sigma} \int_N d\mathbf{y} d\xi d\nu W_a(\mathbf{k}, \mathbf{x}; \mathbf{y}, \xi, \nu) e^{i|\mathbf{k}|\phi_a(\mathbf{x}, \mathbf{y}, \xi, \nu)}, \quad (C8)$$

with

$$\begin{cases} \phi_a(\mathbf{x}; \mathbf{y}, \xi, \nu) = -\nu\tau_d(\mathbf{x}, \xi) + \nu\tau_d(\mathbf{y}, \xi) - \mathbf{n} \cdot \mathbf{y}; \\ W_a(\mathbf{k}, \mathbf{x}; \mathbf{y}, \xi, \nu) = 4|\mathbf{k}|^3 \sigma_0^2(\mathbf{x}) \sigma_0^2(\mathbf{y}) \nu^2 A_d(\mathbf{y}, \xi) A_d(\mathbf{x}, \xi), \end{cases} \quad (C9)$$

where  $\nu = \frac{\omega}{|\mathbf{k}|}$  and lies in  $N$ , and  $\mathbf{n} = \frac{\mathbf{k}}{|\mathbf{k}|}$ .

Under the high-frequency approximation,  $|\mathbf{k}|$  is a large parameter. The above integral can be estimated with the stationary phase theorem. The stationary point is obtained by taking the derivatives of  $\phi_a$  with respect to  $\mathbf{y}$ ,  $\xi$  and  $\nu$  equal to 0. This gives:

$$\begin{cases} \tau_d(\mathbf{x}, \xi) = \tau_d(\mathbf{y}, \xi); \\ \frac{\partial}{\partial \xi} \tau_d(\mathbf{x}, \xi) = \frac{\partial}{\partial \xi} \tau_d(\mathbf{y}, \xi); \\ \mathbf{n} = \nu \nabla_{\mathbf{y}} \tau_d(\mathbf{x}, \xi). \end{cases} \quad (C10)$$

The first two equations are satisfied if  $\mathbf{y} = \mathbf{x}$ . Taking into account the last equation and the definition of  $\nu$ , this gives the equation for the stationary coordinate  $\xi_a$ :  $\nabla_{\mathbf{y}} \tau_d(\mathbf{x}, \xi_a) = \frac{\mathbf{k}}{\omega(v_a)}$ . Multiplying the last equation in eq. (C10) by  $\mathbf{n}$  gives  $\nu_a = \frac{1}{|\nabla_{\mathbf{y}} \tau_d(\mathbf{x}, \xi_a)|} \text{sgn}(\mathbf{n}, \nabla_{\mathbf{y}} \tau_d(\mathbf{x}, \xi_a))$ . The stationary point is then  $\mathbf{y} = \mathbf{x}$ ,  $\xi = \xi_a$  and  $\nu = \nu_a$ . The high-frequency approximation of  $V_a$  is

$$V_a(\mathbf{k}, \mathbf{x}) \simeq \frac{(2\pi)^2 W_a(\mathbf{k}, \mathbf{x}; \xi_a, \mathbf{x}, \nu_0(\mathbf{x}))}{|\mathbf{k}|^2 \sqrt{|\det \hat{\phi}_a|}} e^{-i\mathbf{k}\cdot\mathbf{x}} e^{i\frac{\pi}{4} \text{sgn}(\hat{\phi}_a)}, \quad (C11)$$

where  $\det \hat{\phi}_a$  is the determinant of  $\hat{\phi}_a$ , the second derivative matrix of  $\phi_a$  with respect to  $\mathbf{y}$ ,  $\xi$ ,  $\nu$ .  $\text{sgn}(\hat{\phi}_a)$ , the signature of  $\hat{\phi}_a$ , is the sum of the sign of the eigenvalues of  $\hat{\phi}_a$ . It can be shown, Appendix D, that  $\det \hat{\phi}_a = -\nu_a^2 h^2(\xi_a; \mathbf{x})$  and  $\text{sgn}(\hat{\phi}_a) = 2\varepsilon \text{sgn} \nu_a$ , with  $h$  the Beylkin determinant and  $\varepsilon = \pm 1$ . Substituting the value of  $V_a$  in eq. (C7) and replacing  $\nu$  by  $\frac{\omega}{|\mathbf{k}|}$  gives:

$$\frac{1}{(2\pi)^2} \int_K d\mathbf{k} T(\omega_a(\mathbf{k}), \xi_a(\mathbf{k}), \mathbf{x}) \check{r}(\mathbf{k}) e^{-i\mathbf{k}\cdot\mathbf{x}} = -g(\mathbf{x}), \quad (C12)$$

with

$$T(\omega_a(\mathbf{k}), \xi_a(\mathbf{k}), \mathbf{x}) = i\varepsilon \frac{4(2\pi)^2 \omega_a(\mathbf{k}) \sigma_0^4(\mathbf{x}) A_d^2(\mathbf{x}, \xi_a(\mathbf{k}))}{|h(\xi_a(\mathbf{k}); \mathbf{x})|}. \quad (C13)$$

The left-hand side of eq. (C12) can be interpreted as a pseudo-differential operator applied to the spectrum of  $\check{r}$ . If it is assumed that  $\check{r}(\mathbf{k})$  mainly contains high-frequency terms (i.e. there is a large parameter  $k_l$  such that  $\int_{|\mathbf{k}| < k_l} d\mathbf{k} |r(\mathbf{k})| \ll \int_{|\mathbf{k}| > k_l} d\mathbf{k} |r(\mathbf{k})|$  and that  $\check{r}(\mathbf{x})$  has a compact support), the theory of pseudo-differential operators, Treves (1980), tells us that up to smooth terms the inverse of eq. (C12) is:

$$\check{r}(\mathbf{k}) = - \int_D d\mathbf{y} [T(\omega_a, \xi_a, \mathbf{y})]^{-1} e^{i\mathbf{k}\cdot\mathbf{y}} g(\mathbf{y}). \quad (C14)$$

Substituting  $g$  by its value, eq. (C5), and applying the inverse Fourier transform and the change of variables  $\mathbf{k} = |\omega|\mathbf{p}$  gives

$$\check{r}(\mathbf{x}) = \frac{2i}{(2\pi)^2} \int_{\Sigma} \int_{\Omega} d\xi d\omega \bar{d}(\xi, \omega) \omega^3 V_b(\mathbf{x}, \omega, \xi), \quad (C15)$$

$$V_b(\mathbf{x}, \omega, \xi) = \int_D \int_P d\mathbf{y} d\mathbf{p} W_b(\mathbf{y}, \mathbf{p}, \omega, \xi) e^{i|\omega|\phi_b(\mathbf{x}, \mathbf{y}, \mathbf{p}, \omega, \xi)}, \quad (C16)$$

with

$$\begin{cases} \phi_b(\mathbf{x}, \mathbf{y}, \mathbf{p}, \omega, \xi) = \mathbf{p} \cdot \mathbf{y} - \mathbf{p} \cdot \mathbf{x} + \text{sgn}(\omega)\tau_d(\mathbf{y}, \xi); \\ W_b(\mathbf{y}, \mathbf{p}, \omega, \xi) = \sigma_0^2(\mathbf{y})A_d(\mathbf{y}, \xi)(T(\omega_a, \xi_a, \mathbf{y}))^{-1}. \end{cases} \quad (\text{C17})$$

( $P$  is the space containing  $p$  deduced from  $K$ .)

Under the high-frequency approximation  $|\omega|$  is a large parameter.  $V_b$  can be approximated with the stationary phase theorem. The stationary point, obtained by taking the derivative of  $\phi_b$  with respect to  $(\mathbf{y}, \mathbf{p})$  equal to 0, is  $\mathbf{x}, \mathbf{p}_b$  with  $\mathbf{p}_b = -\text{sgn}(\omega)\nabla_{\mathbf{x}}\tau_d(\mathbf{x}, \xi)$ . The high-frequency approximation of  $V_b$  is

$$V_b(\mathbf{x}, \omega, \xi) \simeq \frac{(2\pi^2)W_b(\mathbf{x}, \mathbf{p}_b, \xi, \omega)}{\omega^2 \sqrt{|\det \hat{\phi}_b|}} e^{i\omega\tau_d(\mathbf{x}, \xi)} e^{i\frac{\pi}{4} \text{sgn}(\hat{\phi}_b)}, \quad (\text{C18})$$

$\hat{\phi}_b$  is the matrix of the second derivatives of  $\phi_b$  with respect to  $\mathbf{y}, \mathbf{p}$ . We have  $\det \hat{\phi}_b = -1$  and  $\text{sgn}(\hat{\phi}_b) = -2\varepsilon \text{sgn} \omega$  (see Appendix D), then

$$V_b(\mathbf{x}, \omega, \xi) = -i\varepsilon \frac{\text{sgn}(\omega)(2\pi)^2 \sigma_0^2(\mathbf{x}) A_d(\mathbf{x}, \xi) (T(\omega_a, \xi_a, \mathbf{x}))^{-1}}{\omega^2} e^{i\omega\tau_d(\mathbf{x}, \xi)}. \quad (\text{C19})$$

From the definitions of  $\omega_a = |\mathbf{k}| v_a = -\omega$  and  $\xi_a$ , this leads to  $T(\omega_a, \xi_a, \mathbf{x}) = -T(\omega, \xi, \mathbf{x})$ . Substituting the value of  $V_b$ , eq. (C19), into eq. (C15) gives the high-frequency approximation of the least-squares solution:

$$\check{r}(\mathbf{x}) = \frac{i}{8\pi^2} \int_{\Sigma} \int_{\Omega} d\xi d\omega \frac{\text{sgn}(\omega) v_0^2(\mathbf{x}) |h(\xi, \mathbf{x})|}{A_d(\mathbf{x}, \xi)} e^{i\omega\tau_d(\mathbf{x}, \xi)} \bar{d}(\xi, \omega). \quad (\text{C20})$$

$\check{r}$  is equal to the ray-based inverse approximation, eq. (18).

#### APPENDIX D: THE MATRICES $\hat{\phi}_a$ AND $\hat{\phi}_b$

The matrices of the second derivatives of  $\phi_a$  and  $\phi_b$  read:

$$\hat{\phi}_a = \begin{pmatrix} v_a \frac{\partial^2 \tau_d}{\partial y_1^2} & v_a \frac{\partial^2 \tau_d}{\partial y_2 \partial y_1} & v_a \frac{\partial^2 \tau_d}{\partial \xi \partial y_1} & \frac{\partial \tau_d}{\partial y_1} \\ v_a \frac{\partial^2 \tau_d}{\partial y_1 \partial y_2} & v_a \frac{\partial^2 \tau_d}{\partial y_2^2} & v_a \frac{\partial^2 \tau_d}{\partial \xi \partial y_2} & \frac{\partial \tau_d}{\partial y_2} \\ v_a \frac{\partial^2 \tau_d}{\partial y_1 \partial \xi} & v_a \frac{\partial^2 \tau_d}{\partial y_2 \partial \xi} & 0 & 0 \\ \frac{\partial \tau_d}{\partial y_1} & \frac{\partial \tau_d}{\partial y_2} & 0 & 0 \end{pmatrix}; \quad (\text{D1})$$

$$\hat{\phi}_b = \begin{pmatrix} -\text{sgn} \omega \frac{\partial^2 \tau_d}{\partial^2 y_1^2} & -\text{sgn} \omega \frac{\partial^2 \tau_d}{\partial y_2 \partial y_1} & 1 & 0 \\ -\text{sgn} \omega \frac{\partial^2 \tau_d}{\partial y_1 \partial y_2} & -\text{sgn} \omega \frac{\partial^2 \tau_d}{\partial^2 y_2^2} & 0 & 1 \\ 1 & 0 & 0 & 0 \\ 0 & 1 & 0 & 0 \end{pmatrix}. \quad (\text{D2})$$

These two matrices are real and symmetric, therefore, their eigenvalues are real. We have  $\det \hat{\phi}_a = -v_a^2 h^2(\xi, \mathbf{x})$  and  $\det \hat{\phi}_b = -1$ . Both determinants are strictly negative. Since the determinant is equal to the product of the eigenvalues, this means that the matrices have either three negative eigenvalues and one positive, or three positive eigenvalues and one negative. The signature of a matrix is the sum of the sign of its eigenvalues, thus the signature of  $\hat{\phi}_a$  or  $\hat{\phi}_b$  is 2 or  $-2$ . The eigenvalues satisfy:

$$\left\{ \left( \frac{\lambda}{\alpha} \right)^2 \left[ \left( \frac{\partial^2 \tau_d}{\partial y_1 \partial y_1} - \frac{\lambda}{\alpha} \right) \left( \frac{\partial^2 \tau_d}{\partial y_2 \partial y_2} - \frac{\lambda}{\alpha} \right) - \left( \frac{\partial^2 \tau_d}{\partial y_1 \partial y_2} \right)^2 \right] \right\} - \beta = 0. \quad (\text{D3})$$

with  $\alpha = v_a$  and  $\beta = \frac{h(\xi, \mathbf{x})}{v_a^2}$  for  $\hat{\phi}_a$  and  $\alpha = -\text{sgn}(\omega)$  and  $\beta = 1$  for  $\hat{\phi}_b$ .  $\frac{\lambda}{\alpha}(\beta)$  is continuous in  $\beta$  and it is equal to 0 if and only if  $\beta = 0$ . Since  $\beta$  is positive for  $\hat{\phi}_a$  and  $\hat{\phi}_b$ , the eigenvalues divided by  $\alpha$  keep the same sign; this means that the number of positive (negative) eigenvalues depend only on the sign of  $\alpha$ .

Then  $\text{sgn}(\hat{\phi}_a) = 2\varepsilon \text{sgn}(v_a)$  and  $\text{sgn}(\hat{\phi}_b) = -2\varepsilon \text{sgn}(\omega)$ , with  $\varepsilon = \pm 1$ .